''Nanosized Voltmeter'' Enables Cellular-Wide Electric Field Mapping

Katherine M. Tyner,*† Raoul Kopelman,† and Martin A. Philbert*
*Toxicology Program and †Chemistry Department, University of Michigan, Ann Arbor, Michigan

ABSTRACT Previously, all biological measurements of intracellular electric fields (E fields), using voltage dyes or patch/voltage clamps, were confined to cellular membranes, which account for <0.1% of the total cellular volume. These membrane-dependent techniques also frequently require lengthy calibration steps for each cell or cell type measured. A new 30-nm ''photonic voltmeter'', 1000-fold smaller than existing voltmeters, enables, to our knowledge, the first complete three-dimensional E field profiling throughout the entire volume of living cells. These nanodevices are calibrated externally and then applied for E field determinations inside any live cell or cellular compartment, with no further calibration steps. The results indicate that the E fields from the mitochondrial membranes penetrate much deeper into the cytosol than previously estimated, indicating that, electrically, the cytoplasm cannot be described as a simple homogeneous solution, as often approximated, but should rather be thought of as a complex, heterogeneous hydrogel, with distinct microdomains.

INTRODUCTION

Electric fields (E fields) are found in and surround every living cell and are critical for the proper functioning of biological processes. These E fields are as widely varied as the high internal fields that preserve cells' energy-dependent nonequilibrium chemical steady state, or the cell-to-cell signaling fields in complex organisms. Biological E fields can affect the entire human body, such as the E fields associated with neural signals or cardiac rhythm. Major E fields are also found in volumetrically small components of cells, such as the mitochondria. The E fields associated with the mitochondrial membrane are relatively large, with a highly polarized inner membrane potential, as high as −150 mV (1,2). Dividing the membrane potential by the distance that the potential spans (the width of the membrane, ~5 nm) produces an E field on the order of -3×10^7 V/m. Changes in E fields can indicate perturbations in biological function, such as observed in Alzheimer's disease (reduction of the E field associated with the neuronal membrane potential (3)) or cell death (loss of the E field associated with the mitochondrial membrane (4)).

Externally applied E fields have been employed in the modulation of a variety of physiological and pathophysiological processes, and significant alteration/adaptation of cellular regulatory processes have been achieved. In the clinical management of wound healing, external E fields have been shown to accelerate repair (5). Both endogenous and applied E fields have been demonstrated to stimulate *Xenopus* nerve growth and regeneration (6). Exposure of cells in culture to short E field pulses induces electroporation of membranes for the delivery of nucleotides, peptides, and small proteins; many of these are under development as therapeutics (7). External E fields have also been shown to induce mitochondria to fuse (8) and to stimulate gene expression (9). However, with available technologies, it remains difficult to assess the effect of external fields on many intracellular components in the live cell.

With both external and internal cellular E fields producing wide-ranging biological effects, the ability to measure complete electric profiles (charge-coupled gradients and fields) of cells will greatly enhance the understanding of biological processes. The measurement of E fields in biology and, in particular, cellular biology has been limited to membrane-dependent methods, be they voltage-sensitive dyes (10–20), patch and voltage clamps (21), green fluorescence protein methods (22), or fluorescence resonance energy transfer techniques (23), i.e., limited to <0.1% volume fraction of the cell.

Despite being generated by the segregation and passage of ions in and through biological membranes, the resulting E fields have profound effects on a variety of nonmembranous functions. However, the distances that such E-fields extend beyond the associated membrane, and the range of their influence, remain largely unmeasured and unknown. As a result, there are today wide gaps in the descriptions of cellular E field profiles, profiles that could greatly enhance current knowledge of cellular organization and signaling. For example, there is a proposed three-dimensional E field signaling network that has the nucleus at the center and extends throughout the entire cell, with the endoplasmic reticulum or actin wires and microtubules forming the network (24). Such a system could not be detected or readily quantified with currently available techniques. In addition to limiting E field characterizations to membranes, the current methods used to measure E fields are often invasive (patch and voltage clamps, microelectrodes), or their measurements exhibit cell-to-cell variation (voltage dyes), resulting in lengthy voltage calibrations or significant inaccuracies (23,25,26).

In this report we describe the design, synthesis, and biological application of a universal, autonomous, wireless,

Submitted June 28, 2006, and accepted for publication March 23, 2007.

Address reprint requests to Raoul Kopelman, Dept. of Chemistry, University of Michigan, 930 N. University, Ann Arbor, MI 48105. Tel.: 734-764-7541; Fax: 734-936-2778; E-mail: kopelman@umich.edu.

Editor: Leslie M. Loew.

0006-3495/07/08/1163/12 $2.00

doi: 10.1529/biophysj.106.092452

nanosized, ''photonic voltmeter''—a nanosensor that is not confined to the exploitation of the properties of lipid bilayers during changes in E fields. These nanoparticles measure E fields with the aid of photons and are called below ''electro-PEBBLEs (E-PEBBLEs)''.

The E-PEBBLEs presented here arise from the previously described PEBBLE (photonic explorer for biomedical use with biologically localized embedding) technology used to measure analytes such as calcium, potassium, nitric oxide, oxygen, etc. inside cultured cells (27) as well as physical properties including viscosity (28). The emergence of E-PEBBLEs allows for the potential use of multiple sensor systems in a living cell to simultaneously determine not only the chemical but also resulting physical properties of biological processes.

A schematic of the E-PEBBLEs is shown in Fig. 1 *A*. The particles encapsulate the fast response voltage-sensitive dye di-4-ANEPPS. The dye's fluorescence spectrum shifts in response to changing E fields (29). This shift can be analyzed ratiometrically, greatly reducing any background noise in the sample (26,30). The dye is encased in the hydrophobic core of a silane-capped mixed micelle, which provides a uniform environment for the molecules. These nanoparticles are universally applicable in the sense that they are calibrated before use and are inserted as calibrated nanoprobes into any cell, cellular compartment, or external region (including non-cellular systems), without the requirement for further calibration. These nanodevices also allow for the measurement of E fields in the cytosol and the ability to construct complete cellular E field profiles through the use of confocal microscopy. This new ability is expected to greatly enhance the understanding of the role of cellular E fields in influencing and/or regulating biological processes, with wider implications for cellular biology, biophysics, and biochemistry.

MATERIALS AND METHODS

E-PEBBLEs synthesis

All chemicals, unless noted, were purchased from Sigma-Aldrich (St. Louis, MO). Triton X-100 (0.625 g, 1 mmol) was dissolved in 10 mL of deionized water. Octyltriethoxysilane (63 μL, 0.2 mmol) was slowly added and the solution allowed to stir for 30 min. Ammonium hydroxide (10–20 μL of a 2.2 M solution) was added, and the solution was stirred for 72 h. Trimethylethoxysilane (200 μL, 1.3 mmol) was added and the solution allowed to stir for an additional 48 h.

The solution was dialysized against water for 24 h in a Spectra/Por polyvinylidene difluoride (PVDF) dialysis membrane (Spectrum Labs, Rancho Dominguez, CA) with a 250-kDa molecular mass cutoff. The bath water was changed three times during the 24-h period. The particle solution was then stirred with an equal volume of a 1 wt % solution of poly (diallyldimethylammonium chloride) (low molecular weight) and again dialyzed for 24 h. Cleaned emulsions were placed on a holey carbon-coated grid (SPI Supplies, West Chester, PA), allowed to dry, and analyzed through transmission electron microscopy (JEOL 3011 high-resolution electron microscope; JEOL, Tokyo, Japan). Solutions of E-PEBBLEs were also analyzed with light scattering using the number-weighted distribution (PSS Nicomp 380 ZLS, Particle Sizing Systems, Santa Barbara, CA).

A 2-mL aliquot of the washed and coated particles was sonicated with a 20-μL solution of di-4-ANEPPS (Molecular Probes, Eugene, OR) dissolved in chloroform (0.1 mg/mL, 0.2 mM). A stirbar was added, and the solution was stirred under an aluminum foil tent for 30 min to remove the chloroform. Solutions were stored in the dark at room temperature and calibrated through use of an external calibration device. Unless otherwise stated, the E-PEBBLEs are used dispersed in the above aqueous stock solution with a concentration of ~5 mg nanoparticles per mL.

E-PEBBLE controls

E-PEBBLE controls were examined in a Horiba (Kyoto, Japan) FluoroMax-3 (excitation 488 nm, emission 500–800 nm, slits 5.00 nm). Emission ratios were constructed by averaging the fluorescent intensity for 50-nm-wide regions. For example, to obtain the 600 nm data point, the average intensity between 575 nm and 625 nm was calculated. Emission ratios analyzed were 600:700 nm and 525:700 nm. Emission spectra of free dye dissolved in organic solvents were taken using approximately the same concentration of dye as found in the loaded nanoparticle solution.

To assess the possibility of reactive oxygen species affecting the E-PEBBLEs performance, the following protocol was followed: A solution of E-PEBBLEs (100 μL stock solution in 3 mL deionized water) was placed in a plastic cuvette and the emission spectrum determined. Hydrogen peroxide (100 μL of a 30 wt % solution, GFS Chemicals, Columbus, OH) was added to the cuvette, and the liquid was pipetted to disperse the E-PEBBLEs. An emission scan was taken immediately and then every 5 min thereafter for 15 min.

The E-PEBBLE's response to different pH solutions was also measured. E-PEBBLEs (50 μL stock solution) were placed into plastic cuvettes. Fisher Buffer Solutions (Fisher Scientific, Hampton, NH) ranging from pH 5 to pH 9 were added to the cuvettes, and the solutions pipetted to disperse the nanoparticles. Emission spectra were taken for each pH.

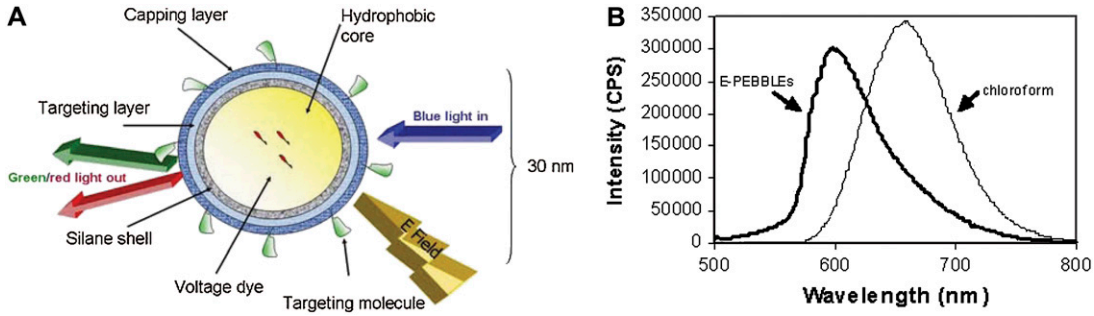

FIGURE 1 Fluorescent E-PEBBLEs. (*A*) Schematic of E-PEBBLEs. The voltage-sensitive dye is encased in a silane-capped micelle. The uniform environment allows the nanoparticles to be calibrated externally before delivery to cells. (*B*) Emission spectra from an aqueous suspension of E-PEBBLEs and a solution of free dye dissolved in chloroform. There is a blue shift in the emission spectrum when the dye is encapsulated inside the nanoparticles (excitation 488 nm).

The effect of different concentrations of dissolved oxygen on the E-PEBBLE's performance was examined as follows: To an air-tight quartz cuvette fitted with a septum and cap, 50 μL E-PEBBLEs stock solution was added along with 3 mL deionized water. N_2 (prepurified, Metro Welding, Detroit, MI) was bubbled through the solution for 10 min, the cuvette was then sealed, and the emission spectrum recorded. Oxygen (USP, Metro Welding) was then bubbled through the solution for 4 min, followed sequentially by air (dry grade, Metro Welding) for 10 min, N_2 for 10 min, and O_2 for 10 min. Emission spectra were taken after each exposure to the gas.

The E-PEBBLEs were also examined to determine if the voltage-sensitive dye leaches out of the nanoparticle matrix over time. A solution of E-PEBBLEs (1.5 mL stock solution) was placed into PVDF dialysis tubing (250 kDa molecular mass cutoff) and the tubing placed into a 300 mL water bath. The bath water was gently stirred. Aliquots of the bath water solution were taken after 15 s of incubation, and then every hour thereafter for 7 h. Aliquots were placed in a plastic cuvette and measured in a Horiba FluorMax-3 spectrofluorometer (parameters as above but with slits of 2.5 nm). After the fluorescent measurement, the aliquot of the bath solution was returned to the bath. After the 7-h time point, an aliquot of the bath water was mixed in a 50:50 ratio with 95% ethanol (AAPER, Shelbyville, KY) to ensure that dye molecules were not leaching from the nanoparticles and forming insoluble and nonfluorescent aggregates. The contents of the dialysis tube were then emptied into the bath solution, stirred and measured to provide the maximum possible fluorescent intensity for the bath solution.

The effect of temperature on a solution of E-PEBBLEs was examined as follows: A solution of E-PEBBLEs (150 μL stock in 3 mL) was placed in a preheated chamber containing a glass coverslip bottom. Temperature measurements and corresponding emission spectra were taken approximately every minute as the solution heated to over 37°C. The chamber was then allowed to cool, and the temperature and emission spectra were again taken until the solution reached room temperature. Emission spectra were taken on an Olympus IMT-II (Lake Success, NY) inverted fluorescence microscope with an Acton Research (Trenton, NJ) spectrograph and a Hamamatsu (Hamamatsu, Japan) HC230 charge-coupled device (CCD) interfaced with an Intel Pentium computer. The CCD was controlled by the software program LABVIEW (National Instruments, Austin, TX). Excitation was from a xenon lamp, and the microscope was fitted with a standard Olympus blue filter cube. Emission ratio values taken during the heating portion of the experiment are labeled with an ''h''. Those values taken during the cooling period are labeled with a ''c''.

Calibration device fabrication

Square glass capillary tubes (inner diameter 52 microns and outer diameter 300 microns) (Polymicro Technologies, Phoenix, AZ) were stripped of their polyimide coating by soaking in concentrated sulfuric acid at 150°C for 5 min. The stripped tubes were then soaked in deionized water for 30 min and finally soaked in 95% ethanol for 30 min. The tubes were allowed to dry overnight.

The stripped tubes were cleaved into small pieces (~5 mm in length) and loaded with E-PEBBLEs by dipping the ends of the tubes into either a solution of the E-PEBBLEs or a dried gel of the nanoparticles. The loaded tubes were affixed to glass coverslips with a thin, clear varnish (Revlon clear 771, Revlon, New York, NY). The varnish was allowed to dry for 30 min before the sides of the tube were painted with silver paint (SPI Supplies) and allowed to dry overnight. Fig. 2 *A* shows a schematic of the external calibration device.

External calibration of E-PEBBLEs

Safety note: Arcing and electrical shock are possible at this step. Appropriate measures to guard against fire and electric shock should be in place before the power supply is connected. The calibration device fabricated above was fixed to the stage of a confocal microscope (Olympus IX70 connected to a Life Science Resources (Cambridge, UK) UltraView equipped with an Ar-Kr laser and a Lambda 10-2 Sutter wheel from Sutter Instrument (Novato, CA)). Wires were connected to the device by painting them to each side of the capillary tube with silver paint. The wires were connected to a power supply (PowerPac HV, Bio-Rad Laboratories, Hercules, CA), and the E field was modulated through the use of the power supply. Voltages were increased by 250-V steps for each measurement, until 1250 V were reached. The voltage was then decreased by 250-V steps until 0 V. The voltage for each data point was allowed to stabilize for 1 min before taking a measurement. The power supply was then allowed to rest at 0 V for 1 min before a new voltage was entered. Devices were not exposed to voltages >1250 V. After this voltage, the devices experienced arcing or shorts in the system. The E-PEBBLEs were excited at 488 nm. Emission images were collected at 600 nm (50 nm bandpass), 700 nm (500 nm bandpass), and 525 nm (50 nm bandpass) with Perkin Elmer (Foster City, CA) UltraView imaging software in Temporal mode.

Calibration image analysis

The images were transferred to the image analysis package MetaMorph (Molecular Devices, Sunnyvale, CA), and rectangular regions of interest (ROI) were chosen spanning the length of the capillary channel, both on the positive and negative sides of the channel. Regions that were noticeable (brighter areas or regions at the edge of a feature) were also selected for analysis. The average pixel intensity for each ROI was calculated. The

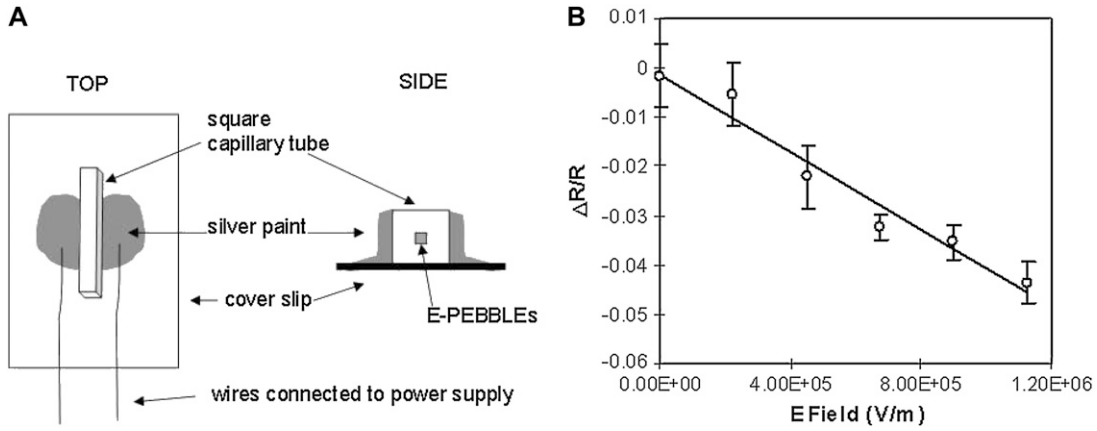

FIGURE 2 Calibration of E-PEBBLEs. (*A*) Schematic for external calibration device. The device is connected to a power supply through the use of wires. (*B*) Representative calibration curve for E-PEBBLEs with error bars of standard deviation ($n = 4$). The best fit line is calculated with linear regression (95% confidence, $r^2 = 0.96$, significance $F = 0.0006$).

emission ratio (R) was then determined using the average pixel intensity values for the 600-nm emission image versus the 700-nm image, or the 525-nm emission image versus the 700-nm emission image. The emission ratio was plotted versus E field. As the glass siding of the capillary tube will diminish the E field across the microchannel where the E-PEBBLEs are located, the E field was calculated by taking the E field at 300 microns (step voltage divided by the width of the capillary tube) and dividing by the dielectric constant of the silica (3.7) as reported in the product literature (31). To eliminate any background fluorescence from the measurements, a ''change in ratio'' (subtracting the ratio (R) at a given E field from the ratio when no E field is present and dividing by R ($\Delta R/R$)) was also calculated and plotted versus E field. At least four trials were completed (two curves with the E field increasing and two curves with decreasing E fields) and used to provide the arithmetic mean and standard deviation before the performance of regression analysis to determine the slope, intercept, and errors of the calibration curve. These values for slope and intercept were used when analyzing cellular systems. A representative calibration curve is shown in Fig. 2 *B*.

Measuring mitochondrial membrane and cytosol potentials

Immortalized rat astrocytes (DITNC) with auto fluorescent mitochondria (American Type Culture Collection, Manassas, VA) (32) were plated onto glass coverslips at a concentration of $\sim 2 \times 10^5$ cells/mL. Cells were incubated in Dulbecco's modified Eagle medium (DMEM) supplemented with 10% fetal bovine serum and 1% penicillin/streptomycin (Invitrogen, Carlsbad, CA) overnight. The media were then removed and replaced with fresh media. E-PEBBLEs (50–100 μL of stock solution) were added to the wells and the cells incubated for 40 min. The coverslip was rinsed with Hanks' balanced salt solution (HBSS) (Invitrogen) containing 10 mmol HEPES and placed in a stainless steel cell chamber with 1 mL HBSS containing 10 mmol HEPES. In some cases tetramethylrhodamine methyl ester (TMRM) (Molecular Probes) dissolved in dimethyl sulfoxide (DMSO) was added to the chamber for a total concentration of $\sim$50 nM to confirm mitochondrial fluorescence.

The entire chamber was mounted on a confocal microscope at room temperature (Olympus IX70 connected to a Life Science Resources UltraView equipped with an Ar-Kr laser and a Lambda 10-2 Sutter wheel from Sutter Instrument) and examined with a 60× objective connected to a Z series motor. Four Z stacks were taken 1 min apart, starting at time zero. At 3 min, 40 s, 1 μL of a carbonyl cyanide 3-chlorophenylhydrazone (CCCP) solution-dissolved DMSO (concentration 12.2 mM) was added to the cell chamber (final CCCP concentration in chamber was 12.2 μM, total DMSO concentration by volume was 0.05%). A Z series of images (1 μm in thickness to allow for future three-dimensional reconstruction) was taken in the vertical plane every minute for 15 min and then every 5 min thereafter until the 30-min time point. Slices analyzed were $\sim$3–4 microns into the cell as measured from the bottom of the cell.

Cells were illuminated at 488 nm, and the fluorescent images were collected at 600 nm (50 nm bandpass), 700 nm (50 nm bandpass), and 525 nm (50 nm bandpass). A fourth channel for TMRM had a 568-nm excitation and an emission of 600 nm (50 nm bandpass). Cells loaded with E-PEBBLEs only, E-PEBBLE matrix without dye (blank), free dye in water (at the same final concentration delivered in the E-PEBBLEs), TMRM only, or cells with nothing added to them provided the panel of controls used in the validation of the E-PEBBLEs. In some cases C6 gliomas were used to further confirm the controls. In addition, some cells exposed to E-PEBBLEs were treated with a HBSS/DMSO solution that contained no CCCP. In some cases, the final polymer coating was not applied and the loaded E-PEBBLEs added directly to the cells.

Repeated depolarizations of mitochondrial membrane potentials

Astrocytes were prepared as described above. Z series of images were taken every minute for 15 min and every 5 min thereafter for 30 min. At time 3 min 50 s, 1 μL of a CCCP solution (3.1 mM dissolved in DMSO and HBSS with HEPES; concentration in chamber was 3.1 μM) was added to the chamber. Starting at the 30-min time point, images were again taken every minute until the 45-min timepoint and every five min thereafter until the 60-min time point. At time 33 min 50 s, a second dose of CCCP (3.1 mM) was added. The final concentration in the cell chamber for CCCP was 6.1 μM.

Cellular image analysis

Images of specific focal planes were transferred to the MetaMorph image analysis package and ROI chosen consistent with TMRM-induced mitochondrial fluorescence or the autofluorescent mitochondria of the astrocytes. In some cases, the images were expanded and ROI were also chosen from the surrounding cytosol. The average pixel intensity was determined for each ROI, and the emission ratio of the 525:700 nm images was then calculated. In some cases the emission ratio of 600:700 nm was calculated. A reference emission ratio was obtained from an area that did not contain a cell but had fluorescent intensity (residual E-PEBBLEs located on the coverslip). This reference point was used as the zero E field and was the value used to calculate $\Delta R/R$. The constructed calibration curve was then utilized to determine E fields. For the TMRM channel, the average pixel intensity was recorded.

RESULTS

Synthesis and characterization

The nanosized sensors are composed of silane-capped mixed micelles that contain the ratiometric, fast response voltage dye di-4-ANEPPS (Fig. 1 *A*). The nanoparticles are synthesized using a modified method of Das et al. (33). The particles contain a hydrophobic core composed of the organic chains of the organosilanes. The micelle is stabilized by polymerizing the silane headgroups. A monoethoxysilane is then added, capping off any unreacted silane groups to prevent aggregation of the particles. Additional silane or polymer layers may be added at this step for enhanced targeting or biocompatibility of the particles. The voltage dye is encapsulated into the organic core of the particle, where it is stabilized in a uniform environment, allowing for universal calibration. Nanoparticles excited at 488 nm produce a broad emission spectrum, ranging from 500 nm to 800 nm, with the emission peak blue shifted from that of the free dye dissolved in chloroform (Fig. 1 *B*). In addition, the emission spectrum narrows as the dye molecules enter the particle ($\sim$15 nm less than the corresponding free dye in chloroform, full width half-maximum). Although not strictly monodisperse, E-PEBBLEs have a mean hydrodynamic diameter that is fairly tightly distributed around 30 nm as determined by transmission electron microscopy (Fig. 3 *A*) and light scattering (Fig. 3 *B*).

The particle solution dries to a gel, and either the aqueous suspension or the gel itself is placed into an external calibration device. The E field the particles are exposed to may be modulated through use of a power supply connected to the external device by wires. As the E field experienced by the nanoparticles increases, the emission ratio (calculated from the emission intensity at 525 nm and 700 nm, excitation 488 nm) of the embedded dye decreases. The raw curves are

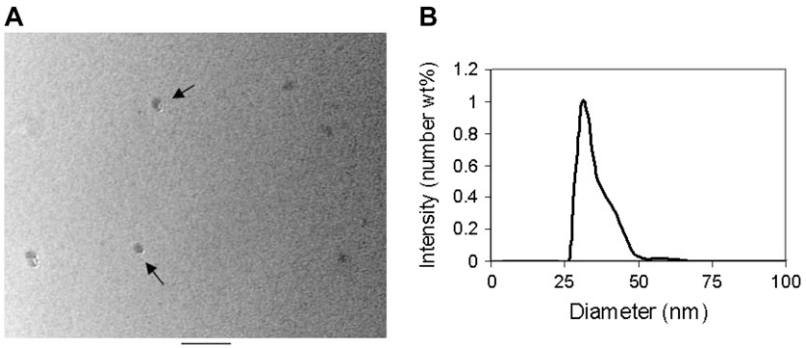

FIGURE 3 Size characterization of E-PEBBLEs. (*A*) Transmission electron microscopy image of E-PEBBLEs. The scale bar is equal to 100 nm. The particles are ~30 nm in diameter (*arrows* pointing out individual particles). (*B*) Number-weighted light scattering data for E-PEBBLEs.

then transformed into ''change in emission ratio over emission ratio'' ($\Delta R/R$) by subtracting the emission ratio at a certain E field from the emission ratio when there is no E field present and the slope and *y* intercept calculated using regression analysis with 95% confidence ($r^2 = 0.96$, significance $F = 0.0006$). The slope and *y* intercept for the batch of E-PEBBLEs used in this report was -3.9×10^{-8} V/m and -0.001, respectively. These values from the external calibration are then used to determine the E fields inside cells, without having to calibrate individual sensors within the cells themselves. ROI from both the positive and negative sides of the channel inside the calibration device are examined as well as any other noticeable feature (i.e., bright portions of the tube). There does not appear to be any migration of the nanoparticle gel, either in the form of uneven changes in fluorescent intensity or movement of the gel out of the ROI, during the application of the E fields, indicating that the optical response arises solely from the electrochromatic changes of the dye itself.

E-PEBBLEs controls

E-PEBBLEs exposed to hydrogen peroxide, a range of pH solutions, or varying oxygen concentrations showed no noticeable change in the corresponding emission ratios (data not shown). E-PEBBLEs incubated in a water bath for 7 h showed no evidence of the dye molecules leaching out of the nanoparticles (Fig. 4). Adding ethanol to the bath water to probe for insoluble and nonfluorescent aggregates produced no fluorescent response.

Monitoring the emission ratio of 600:700 nm, we found a reversible temperature dependence for the E-PEBBLEs. This emission ratio reversibly decreases with increasing temperature (Fig. 5 *A*). However, using a different portion of the broad emission spectrum eliminates the temperature effects: The emission ratio of 525:700 nm does not show any temperature dependence (Fig. 5 *B*). There is only a slight increase of the emission ratio over the time course of the experiment, most likely due to the evaporation of water and the subsequent concentration of the E-PEBBLE solution. Fig. 5 *C* compares the fluorescent spectra of the E-PEBBLE solution at 35°C and 27°C.

Monitoring mitochondrial E fields using E-PEBBLES

DITNC astrocytes, a model cell line with well-characterized respiratory profiles, were able to take up and tolerate the nanoparticles without further modification. Cells were challenged with the uncoupler CCCP, a chemical that causes rapid dissipation of the E field associated with the mitochondrial membrane. ROIs were determined by locating areas of bright, punctuated fluorescence correlating spatially with mitochondrial fluorescence. The E-PEBBLEs emission ratio was then determined at the measurement time points. A reference emission ratio was obtained from an area that did not contain a cell but had fluorescent intensity (residual E-PEBBLEs located on the coverslip). This reference point was used as the zero E field and was the value used to calculate $\Delta R/R$. Once the measurements were converted to $\Delta R/R$, the values extracted from the external calibration curve were used to determine the E field at the ROI. Fig. 6 *A* shows the E field of a mitochondrial region over time.

In Fig. 6 *A*, at times 0–3 min, before the addition of CCCP, the mitochondrion should be fully polarized, with a large E field. The measured E field value is -3.3×10^6 V/m, which

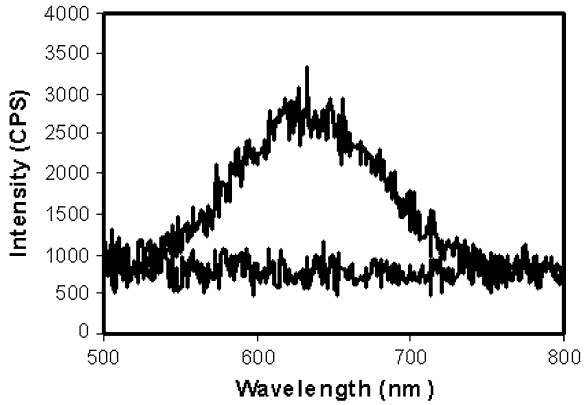

FIGURE 4 Emission spectra from a water bath exposed to a dialysis tube containing stock E-PEBBLEs. The bottom line is the emission spectrum for a water bath exposed to an E-PEBBLEs solution for 7 h. The top spectrum is the total possible emission intensity for the experimental setup (contents of dialysis tube placed into water bath). There is no evidence of the dye leaching out from the nanoparticles, even after 7 h incubation.

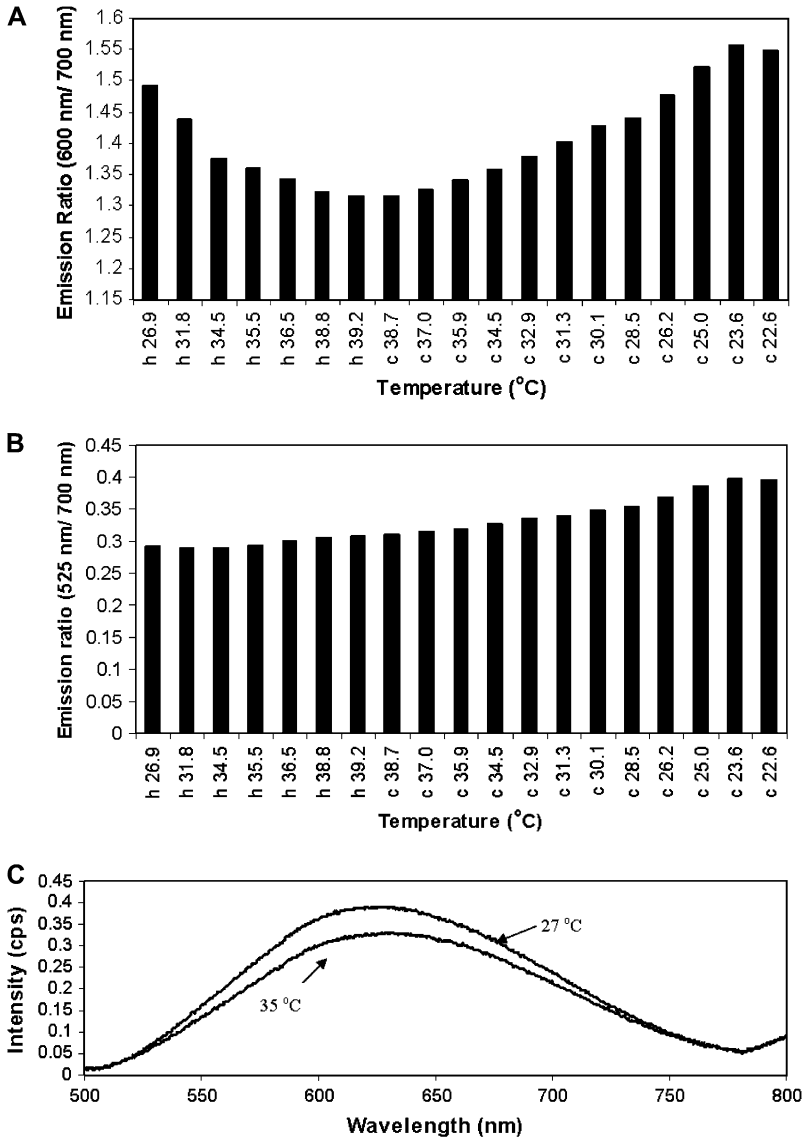

FIGURE 5 Partial temperature dependence of E-PEBBLEs. Bar graphs detail both the heating (h) and cooling (c) cycle of an E-PEBBLEs solution. (*A*) Emission ratio of 600:700 nm. There is a reversible decrease in the emission ratio with increasing temperatures. (*B*) Emission ratio of 525:700 nm for the same data set. There is no temperature dependence for this emission ratio. The slight increase in the emission ratio over the time course of the experiment is most likely due to the E-PEBBLEs solution becoming more concentrated as water evaporates from the solution. (*C*) Comparison between fluorescent spectra taken at 35°C and 27°C.

is lower than the value for a normal, polarized mitochondrion (-3×10^7 V/m) (1,2). The E field is fairly stable, as measured by the E-PEBBLEs. After the addition of CCCP, the E field rapidly decreases. There then follows a slight repolarization of the mitochondrial membrane. This experiment demonstrates the ability of the localized E-PEBBLEs to follow fluctuations in the E field produced by a cellular component, in this case the E field associated with the mitochondrial membrane.

Fig. 6 *B* shows the comparison between cells exposed to CCCP and cells exposed to a control dose of DMSO. Focus is placed on the data points of minutes 3 and 4, the time points taken immediately before and after the addition of CCCP (or the corresponding control of DMSO) at time 3 min 40 s. For the cells exposed to CCCP, the E field at $t = 4$ min is -1.4×10^6 V/m, a drop in E field of 55% from the data taken at minute 3 (-3.1×10^6 V/m), immediately preceding the addition of the poison. In four repeated experiments, the decrease between time points 3 min and 4 min has been as high as 90% and has never been lower than the 55% presented. The overall drop in E field from $t = 0$ min to $t = 30$ min is also 55%. In comparison, there is no drop in E field between time points 3 and 4 for the controlled data of DMSO. There is a slight increase in E field (14%), a result much different from the rapid decrease in E field in the data set containing the CCCP. The control data set has an overall decrease in E field (from $t = 0$ min to $t = 30$ min) of 29%.

In addition to the abrupt change in E field, which can be observed in Fig. 6 *A*, there is also an abrupt change in fluorescent intensity (decrease) in the cells when the CCCP is added. Neither the abrupt change in E field nor the decrease in fluorescent intensity is observed when the control dose of DMSO is added to the cells. There is neither an abrupt change in E field or fluorescent intensity in four repeated

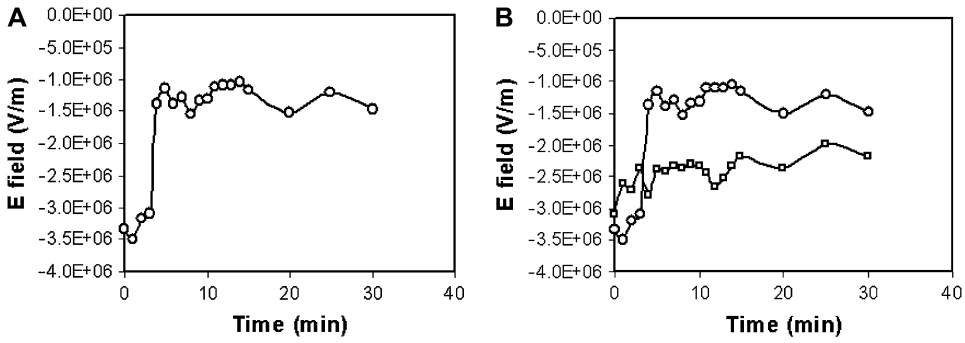

FIGURE 6 E-PEBBLEs follow E fields associated with the mitochondrial membrane. (*A*) E field associated with a mitochondrial membrane versus time as monitored by E-PEBBLEs. The E field of the membrane rapidly decreases after the addition of CCCP at time 3 min and 40 s. (*B*) Comparison of the change in E field for a mitochondrial membrane using E-PEBBLEs. Either CCCP (*circles*) or DMSO (*squares*) is added to the cells at 3 min and 40 s. When CCCP is added, a large change in the E field is immediately observed. When just DMSO is added, however, the E-field remains relatively steady (with, at most, a minor increase initially, followed by a slight depolarization).

trials comparing the effects of CCCP versus the control dose of DMSO (note: in some cases, the repeated trials contained an additional tracking dye or all of the liquid volumes in the chamber were doubled).

Monitoring multiple E-field fluctuations with the temperature-sensitive ratio

Astrocytes were incubated with E-PEBBLEs and transferred to a confocal microscope, and the mitochondrial membrane E field was reduced with a small dose of CCCP. The mitochondria were then allowed to repolarize briefly, and a second dose of CCCP was applied. Fig. 7 shows the E field as a function of time for a mitochondrial region monitored by E-PEBBLEs using the 600:700 nm temperature-sensitive ratio (note: calibration curve used for determining E fields was constructed using the 600:700 nm emission ratio). After the application of the CCCP, the E field rapidly decreases, followed by a modest repolarization. The cells are then exposed to a second dose of CCCP. Again, there is a rapid decrease in the E field, followed by a repolarization. Following the E field using the 525:700 nm temperature-insensitive ratio produced similar trends (data not shown). The E-PEBBLEs followed the multiple changes in the mitochondrial E field for all applications of CCCP in all repeated trials (including trials using different concentrations of CCCP). These results demonstrate the E-PEBBLEs ability to monitor multiple E field fluctuations, even when using a temperature-sensitive emission ratio.

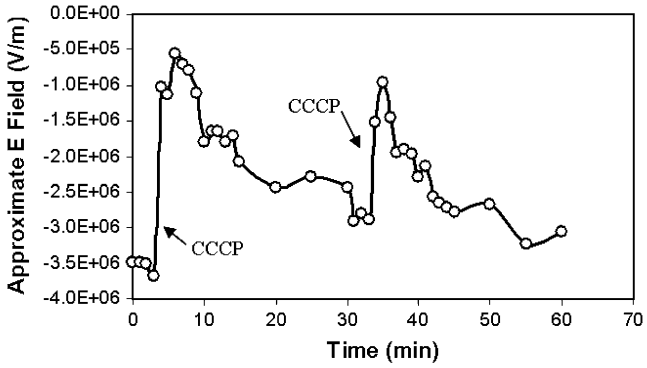

FIGURE 7 E-PEBBLEs follow multiple E field changes. After CCCP is added at time 3 min 50 s and time 33 min 50 s (*arrows*), a rapid loss of the E field associated with a mitochondrial region is observed, followed by a modest repolarization. Note that the E field values are only approximate, as the 600:700 nm emission ratio is being used.

Determining cytosolic E-fields

Fig. 8 *A* shows astrocytes incubated with E-PEBBLEs. The nanoparticles are taken up by the cells and localize throughout the cell but are excluded from the nucleus. Mitochondria appear as bright punctuated regions, whereas E-PEBBLEs have diffuse fluorescence (Fig. 8 *B*). An enlarged region of the middle cell in the image (Fig. 8 *B*) shows ROI containing both mitochondrial regions (regions 5–10) and cytosolic regions (regions 1–4). The E field for all of these ROI was determined using the external calibration curve (Fig. 8 *C*). The E field associated with the mitochondrial membrane drops significantly and rapidly with distance from the polarized mitochondrial membrane (region 5). However, the spatial picture is complicated by the presence of mitochondria above and below the plane of analysis. As the ROI crosses other mitochondrial regions (regions 6–10), the E field again increases. Although the E field intensity never again achieves the maximal intensity measured for the in-plane mitochondrion, the E field is still measurable several microns away from the mitochondria. The E-PEBBLEs have measured E fields extending away from the mitochondria and into the cytosol in over five separate trials.

DISCUSSION

A schematic of the E-PEBBLEs is shown in Fig. 1 *A*. The fast response, voltage-sensitive dye di-4-ANEPPS is

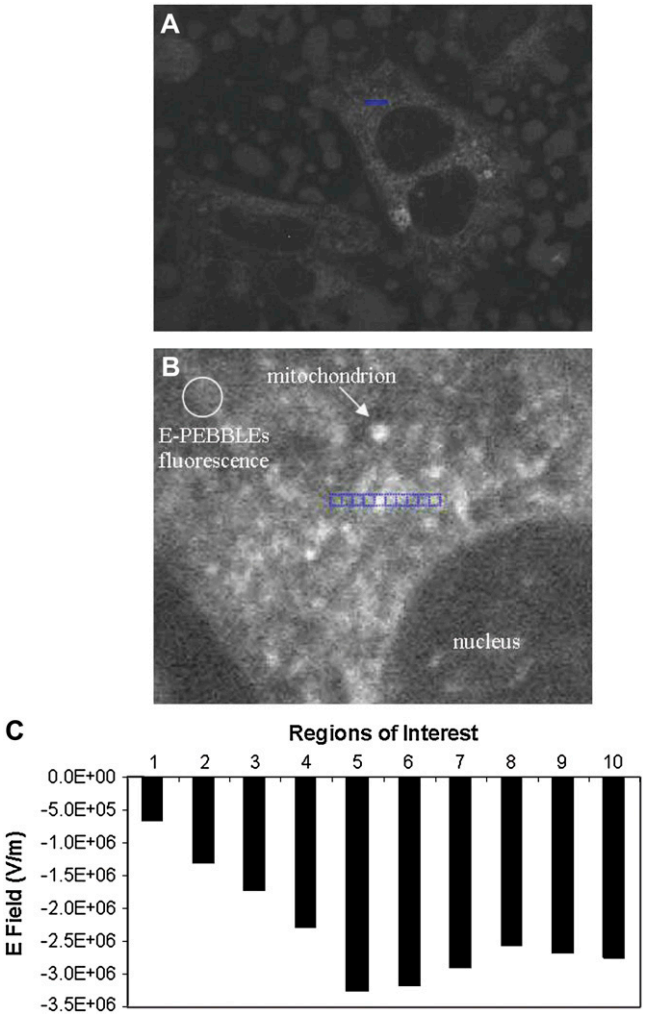

FIGURE 8 E-PEBBLEs can measure E fields in both cytosolic and membrane regions of living cells. (*A*) Astrocytes incubated with E-PEBBLEs. The middle cell contains the region analyzed (*blue line*, 4.5 microns). (*B*) An enlarged image of the cellular region analyzed (both membrane and cytosolic regions). An arrow points out a representative mitochondrion. The circular region contains diffuse fluorescence arising from the E-PEBBLEs. The blue line contains the regions analyzed. The regions are numbered 1–10 from left to right. Region 5 contains a mitochondrion (*brightly fluorescent region*), whereas regions 6–10 cross over other mitochondrial regions. The total length of the ROI is 4.5 microns. The brightness and contrast of this image has been adjusted to 68% and 83% (from 50%, Microsoft Publisher), respectively, for added clarity. (*C*) A graph showing the E field for the ROI before the addition of CCCP. The highest E field is seen in region 5. Emission ratio 525:700 nm.

embedded in the organic core of a mixed micelle formed from a long-chain organosilane and surfactant. The silane headgroups are polymerized to form a thin silane shell around the micelle, which stabilizes the particle. A second silane layer containing a primary amine may be added at this point to allow for the bioconjugation of targeting molecules (targeting layers and targeting molecules are not included in the reported particle and are not discussed in this article). A final silane-capping layer composed of a monoethoxy silane is then added to react with any excess silane headgroups. This capping layer prevents aggregation of the particles. Surfactant and excess silane is removed from the particle solution with dialysis. For the presented sensors, an additional exterior coating of poly(diallyldimethylammonium chloride) is applied to the nanoparticles to allow for cellular uptake.

The dye is depicted to be localized inside the oily core of the nanoparticle. As the dye is hydrophobic, it will preferentially localize into the organic regions of the nanoparticle solution. The dye experiences a blue shift in the emission peak as it goes from a free dye dissolved in chloroform to being encapsulated inside the nanoparticle. This blue shift is similar to the emission shift that occurs when the free dye is bound to a membrane (34). The dye molecules are shown oriented in an E field due to the fact that there is not an observed isotropic cancelling of the dye's fluorescent emission response when the E field changes. The actual orientation of the dye molecules is unknown, and the schematic represents only one possible arrangement of the dye molecules.

Using a fast response, voltage-sensitive dye that is internally ratiometric (i.e., no reference dye is needed to form the ratio) provides several advantages, even when not encapsulated in a nanoparticle matrix. Such advantages include reduction in motion artifacts, noise cancellation of laser and experimental fluctuations, normalization for differences in local sensitivity, photobleaching correction, and enhanced voltage sensitivity (26,30). When the dye is encapsulated in a uniform nanoparticle matrix, the dye's response is further enhanced as fluctuations that occur in the cell and would affect the free dye (membrane rearrangement, fluidity changes, etc.) are eliminated. The uniform environment allows the particles to be calibrated externally and applied to cells or cellular compartments with no further calibration steps.

The calibration curve for the E-PEBBLEs does not encompass the higher cellular E field values. This omission is due to the intricacies of producing the enormous cellular E field outside of cells. The calibration method presented here proved to be the most robust one tested, allowing for the measurement of E fields of $\sim 1.4 \times 10^6$ V/m in strength. Attempts to increase the E field above this value resulted in arcing (electrical breakdown) and the glass device melting onto the microscope objective. Due to the construction methods of the device, significant variation in the calibration slope can sometimes be obtained due to flaws in the capillary tube, but the calibration trends are similar. Current investigations are underway to construct a device that will permit higher E fields with less variance in the data obtained.

Although the calibration curve does not extend into the highest regions of cellular E fields, we expect that the E-PEBBLEs will maintain their linearity throughout the cellular E field range. Studies on the linearity of di-4-ANEPPS or a structurally similar dye (di-8-ANEPPS) show that the emission ratio produces a linear response from -2.4×10^7

V/m to 1.2×10^7 V/m in a variety of environments, ranging from isolated neurons to intact hearts (26,30).

There is an ~0.04 change in the emission ratio from 0 V/m to 1.13×10^6 V/m. Knisley et al. report an ~0.001 change in ratio per 1.13×10^6 V/m (assuming a linear calibration curve) for free dye embedded in the heart tissue (30). This larger change in the E-PEBBLEs emission ratio is likely due to the absence of cellular artifacts or internalization of the free dye by the cell.

We note that the E-PEBBLEs were found to be insensitive to pH, O_2 gradients, or reactive oxygen species (as tested by H_2O_2). Leaching studies indicate that the dye remains in the hydrophobic core of the nanoparticle, thus providing a sensor that is stable over the lifetime of the cellular experiment in various environments.

E-PEBBLEs containing di-4-ANEPPS can be temperature sensitive, depending on the portion of the fluorescent spectrum utilized (Fig. 5). Such temperature-dependent phenomena have also been observed for excitation ratios of several voltage-sensitive dyes. Clark et al. note a temperature dependence for di-8-ANEPPS (35), a structurally similar dye to di-4-ANEPPS, near the emission maximum of the molecule (~580 nm). By utilizing the very broad emission spectrum of di-4-ANEPPS (Fig. 1 *B*), temperature-insensitive emission ratios may be formed. Specifically, using an emission ratio of 525:700 nm eliminates any temperature dependence from the E field measurements. As an experiment may be devised to encompass both the temperature-sensitive and -insensitive regions of the E-PEBBLEs spectrum, there arises the possibility of using the E-PEBBLEs as both E field and temperature sensors simultaneously. Even though parts of the emission spectrum are temperature sensitive, these emission ratios may still be utilized to determine relative changes in the E field (Fig. 7). Alternatively, if the temperature is kept constant, E field values may be extracted from the temperature-sensitive regions by first taking into account the temperature effect on the emission ratio. There are some advantages (described below) to using the 600:700 nm emission ratio. Since the 600:700 nm emission ratio is constructed using emission intensities taken from the top and side of the fluorescent emission peak, there is more fluorescent intensity and a lowering of the signal/noise ratio. As a result, the data obtained from the 600:700 nm ratio, although temperature sensitive, tend to be less noisy than the data extracted from the temperature-insensitive data of the 525:700 nm emission ratio, which is constructed using emission intensity from the sides of the emission peak. If the temperature of the experiment is carefully controlled, or if only relative changes in the E field are desired, the 600:700 nm selection is a convenient emission ratio to use.

The nanoparticles may be used to track changes in E fields associated with organelles, in this case, mitochondria. Fig. 6 shows the E field associated with a mitochondrion before and after the addition of CCCP. Before the addition of CCCP, the E field is $\sim -3.3 \times 10^6$ V/m, which is almost an order of magnitude lower than a fully polarized inner mitochondrial membrane. This result may be explained by the fact that the E-PEBBLEs are not actually inside the inner mitochondrial membrane. The E-PEBBLEs themselves may be adjacent to the mitochondrial outer membrane or simply close to the mitochondria. Repeating the above experiment several times, as well as analyzing different mitochondrial regions in the same cell, produces varying E fields (although the depolarization trend after the addition of CCCP is similar for all of the experiments). The E-PEBBLEs, in contrast to a naked voltage dye, can be at varying distances from the mitochondria. Thus, the resulting lower E field values could be due to the E field diminishing as it passes through the cell to the E-PEBBLEs. In addition, the mitochondria themselves may be in different respiratory, and hence different E field, states.

The E-PEBBLEs localize throughout the cell but are excluded from the nucleus, as indicated by the diffuse fluorescence present in the cells after coincubation with the E-PEBBLEs (Fig. 8 *A*, punctuated brightness is from autofluorescent mitochondria). Due to their relatively small size, the exact location of individual particles cannot be determined with the confocal microscope setup. Colocalization studies indicate that some, but not all, of the particles are in the lysosomes of the cell (data not shown). EM studies to determine nanoparticle distribution proved inconclusive, as the membrane is slightly damaged during nanoparticle entry (as indicated by PI staining), causing cells to rupture during fixation. Although the cellular membrane is damaged by nanoparticle entry, there are viable cells present, even after 48 h of constant incubation with the nanoparticles as determined by assay and examination with a fluorescent microscope (data not shown). Cell groups that appeared visually robust (i.e., elongate with little or no ruffling or blebbing of the membrane) were used for analysis.

After the CCCP is added to the cells, there is a rapid decrease in the E field that is not observed when only DMSO is added to the cells. As the dose of CCCP is relatively small (total concentration in the chamber is 12.2 μM), the E field associated with the mitochondrial membrane does not go to zero. In addition, the E field does not remain at the lower E field value but can increase over time, indicating a repolarization of the mitochondrial membrane.

A control dose of only DMSO does not produce the dramatic decrease in mitochondrial E field as seen with the corresponding application of CCCP. There is a slight decrease in E field over the entire time course of the experiment. The decrease of the E field may be partly due to photobleaching of the dye or the cells themselves becoming stressed as a result of the experimental conditions (over half an hour on an unheated stage in physiological buffer). In addition, since the nanoparticles do slightly damage the cells as indicated by PI staining, this damage may be showing up as a decrease in the mitochondrial E field.

The E-PEBBLEs have several advantages over other methods used to determine E fields associated with organelles in intact cells. Although TMRM and other voltage-dependent

free dyes are used widely to both visualize and characterize E field changes of mitochondrial membranes, these dyes are often in the class of ''slow response dyes''. The positively charged molecules of a slow response dye physically translocate across the mitochondrial membrane, in response to changing E fields. With higher E fields, more dye molecules move across the membrane toward the more negative regions of the cell (mitochondria). When the CCCP decreases the E field associated with the mitochondrial membrane, the molecules can ''leak'' out of the mitochondria, as the strong negative region has dissipated. Since this mechanism involves molecules physically moving across membranes, it can be a slow process. Indeed, depending on concentration and local conditions, the dye may take several minutes to respond to significant E field changes. Di-4-ANEPPS, however, is a fast response voltage dye. The fast response class of molecules embeds within the lipid bilayer itself and changes its fluorescence spectra due to changes in the local environment (electrochromatic changes, orientation, aggregation, etc. (36)). Di-4-ANEPPS exhibits electrochromatic changes in response to changing E fields (29). Due to the fact that the fast response dyes undergo only small changes, these dyes respond within milliseconds to changing E fields. The fast response property of the dye, even when embedded within the particles, allows for the identification and isolation of rapid fluctuations in the mitochondrial membrane potential and should provide a substantial improvement in the ability to measure temporal changes in a variety of other cellular and nonbiological systems. Note that with both classes of free dyes, the traditional molecules, and hence the E field measurements, are confined to the membranes, either by direct embedding or by translocating across the lipid bilayers. Thus, E fields extending into nonmembrane regions of the cells or membranes that are difficult to stain with voltage dyes cannot be measured. In contrast, as the E-PEBBLEs are self-contained units, they can report any E fields throughout the entire cell. Although the dye molecules are possibly no longer oriented the way they are in a biological membrane, the nanoparticles still show an optical response to changing E fields, possibly due to the fact that the organic core of the particle allows for some type of orientation of the molecules in an E field.

Cells exposed to free dye in an aqueous solution did not fluoresce, providing compelling evidence that the dye must be incorporated into the nanoparticles to be taken up by the cells. Controls of E-PEBBLEs with no dye incorporated into the particles, or cells with nothing added to them, did not show a response to changing E-fields.

The E-PEBBLEs not only track E field changes rapidly but can also track multiple E field fluctuations. As a mitochondrion is repeatedly challenged with small doses of CCCP (a quarter of the concentration used in the preceding experiment), the E-PEBBLEs register first the drop in the E field and, subsequently, the repolarization of the E field (Fig. 7). The repolarization is possibly due to the small doses of CCCP or a subsequent ''wash-out'' effect. The same happens even when a temperature-sensitive emission ratio is used. This result demonstrates the E-PEBBLEs' ability to track multiple changes in the E field during a time course experiment. In addition, the particles may be selectively targeted to different regions of the cell, simply based on the exterior coating of the particles (data not shown).

From the above results it becomes clear that, in contrast to the traditional methods, the E-PEBBLEs may be used throughout the entire cell volume instead of being confined to the membrane regions. Thus the above results demonstrate the ability of the nanoparticles to measure E fields outside of the lipid bilayers, whereas all voltage dye and patch-clamp techniques are constrained to measurements inside the membranes. If microelectrodes were used to measure nonmembrane-bound potentials, they would have first to puncture the external membrane (37). In addition, the electrodes do not have the ability to measure multiple regions simultaneously (and also require reference electrodes). Thus the E-PEBBLEs significantly increase the kind and amount of E field information obtainable from cells.

The data shown in Fig. 8 demonstrate the potential of the E-PEBBLEs to provide cellular-wide E field maps containing electrical information that originates from both membrane and nonmembrane regions in individual or multiple optical slices arising from confocal imaging that can be reconstructed for a three-dimensional E field profile. The E field increases sharply as the ROI in the cytosol region approach the mitochondrion in region 5. The E field then slightly dissipates as the ROI extend back into the cytosol. The E-PEBBLE technique is sensitive enough that the E fields arising from mitochondria in a lower focal plane are also observed (regions 6–10). The E-PEBBLEs coupled with confocal microscopy thus provide, for the first time to our knowledge, a method to construct a complete electrical profile of a living cell, spanning both membrane and nonmembrane regions. Analyzing regions far away from mitochondrial regions still produces an E field value, supporting the picture of an electrically complex environment inside the cell.

Due to the limitations of the previous technology, the answer to the question ''How far does a membrane's E-field extend into the cell's interior?'' could only be calculated, not tested experimentally. Such calculations, using as a model a saline solution, indicate that the E fields arising from membranes can extend only 1–10 nm beyond the membrane (38,39). However, the new E-PEBBLE measurements show E fields extending out much farther (microns) into the cytosol. The discrepancy can easily be explained as arising from the choice of the theoretical model. A saline solution may not be the best choice as a cellular model, because the cell's interior (i.e., the cytoplasm) is far from being a simple ionic solution. A better model choice would start with a complex fluid. Indeed, there have been reports indicating that the structure of the cytoplasm is gel-like (40) rather than a simple solution. Studies have also demonstrated that the

forces extending out from the membrane surfaces can cause long-range ordering effects. The latter cannot be explained by simple electrostatics (41). Furthermore, there have been reports of bioelectrical signals that are not confined to the membranes and can extend into the cytosol (6).

In addition to the potentially complex ordering that surrounds lipid bilayers within the cell, there may be other E fields present in the cytosol that could account for the E fields that were measured in the cytoplasm. Such E fields may arise from electrically active membranes of other organelles, the plasma membrane, or regions of the cell's interior that could not be measured with previous techniques, due to either the small size of the objects or for lack of a lipid bilayer into which voltage dyes could be embedded. Ongoing studies using E-PEBBLEs have measured E fields arising from the plasma membrane as well as microfilaments (data not shown). Indeed, microtubules and microfilaments have both been shown to behave as cellular electrical transmission lines that could provide an electrical signaling mechanism throughout a cell (42,43). Confocal studies probing for such E fields and how they interact with the mitochondria are currently underway.

CONCLUSIONS

This article describes the synthesis, characterization, and utilization of a universal, wireless, nanosized, autonomous, ''photonic voltmeter'' and also presents, to our knowledge, the first complete E field imaging of a live cell. The new voltage-sensitive nanoparticles are able to detect fluctuations of E fields throughout the entire cell, including nonmembrane regions. The use of these particles opens up the potential for the determination, with three-dimensional spatial and temporal resolution, of biological sequelae resulting from modulation of hitherto immeasurable E fields that extend into the cytosol and other regions of the cell. These new nanosensors greatly enhance the potential for integrating real-time measurements of intracellular/extracellular E-fields with investigations of voltage-dependent cellular processes that are not immediately proximal to polarized membranes. Such imaging of the entire cell's E fields can now also be integrated with chemical and physical imaging of the live cell, resulting in real high-dimensional images of cells, including multiple physical (space, fields, temperature, viscosity) and chemical (ions, molecules, radicals) dimensions. Furthermore, these first ''nanosize voltmeters'' also open the way for wireless E-field profiling, with minimal ''cross talk'', inside micro/nanoelectronic devices.

The authors thank Jeff Anker for discussions on the feasibility of the design concept and Ron Smith for remote spectroscopy assistance. We also thank the Kyung-Dall Lee laboratory in the College of Pharmacy, University of Michigan, for use of their particle size analyzer.This work was supported by the Defense Advanced Research Project Agency BioMagnetics program (R.K. and M.P.), National Institutes of Health-ES 08846 (M.P.), National Science Foundation DMR-0455330 (R.K.), and National Science Foundation DMR-0315633 (TEM images).

REFERENCES

1. Loew, L. M., R. A. Tuft, W. Carrington, and F. S. Fay. 1993. Imaging in five dimensions: time-dependent membrane potentials in individual mitochondria. *Biophys. J.* 65:2396–2407.
2. Nicholls, D. G., and M. W. Ward. 2000. Mitochondrial membrane potential and neuronal glutamate excitotoxicity: mortality and millivolts. *Trends Neurosci.* 23:166–174.
3. Blanchard, B. J., V. L. Thomas, and V. M. Ingram. 2002. Mechanism of membrane depolarization caused by the Alzheimer Aβ1–42 peptide. *Biochem. Biophys. Res. Commun.* 293:1197–1203.
4. Kim, J. S., L. He, and J. J. Lemasters. 2003. Mitochondrial permeability transition: a common pathway to necrosis and apoptosis. *Biochem. Biophys. Res. Commun.* 304:463–470.
5. Ojingwa, J. C., and R. R. Isseroff. 2003. Electrical stimulation of wound healing. *J. Invest. Dermatol.* 121:1–12.
6. McCaig, C. D., A. M. Rajnickek, B. Song, and M. Zhao. 2005. Controlling cell behavior electrically: current views and future potential. *Physiol. Rev.* 85:943–978.
7. Ghartey-Tagoe, E. B., J. S. Morgan, K. Ahmed, A. S. Neish, and M. R. Prausnitz. 2004. Electroporation-mediated delivery of molecules to model intestinal epithelia. *Int. J. Pharm.* 270:127–138.
8. Reynaud, J. A., H. Labbe, K. Lequoc, D. Lequoc, and C. Nicolau. 1989. Electric field-induced fusion of mitochondria. *FEBS Lett.* 247:106–112.
9. Blank, M., and L. Soo. 2003. Electromagnetic acceleration of the Belousov-Zhabotinskii reaction. *Bioelectrochemistry.* 61:93–97.
10. Buhler, R., W. Sturmer, H. J. Apell, and P. Lauger. 1991. Charge translocation by the Na,K-pump: I. Kinetics of local field changes studied by time-resolved fluorescence measurements. *J. Membr. Biol.* 121:141–161.
11. Zhang, J., R. M. Davidson, M. D. Wei, and L. M. Loew. 1998. Membrane electric properties by combined patch clamp and fluorescence ration imaging in single neurons. *Biophys. J.* 74:48–53.
12. Burgstahler, R., H. Koegel, F. Rucker, D. Tracey, P. Grafe, and C. Alzheimer. 2003. Confocal ratiometric voltage imaging of cultured human keratinocytes reveals layer-specific responses to ATP. *Am. J. Physiol. Cell Physiol.* 284:C944–C952.
13. Shoham, D., D. E. Glaser, A. Arieli, T. Kenet, C. Wijnbergen, Y. Toledo, R. Hildesheim, and A. Grinvald. 1999. Imaging cortical dynamics at high spatial and temporal resolution with novel blue voltage-sensitive dyes. *Neuron.* 24:791–802.
14. Gogan, P., I. Schmiedel-Jakob, Y. Chitti, and S. Tyc-Dumont. 1995. Fluorescence imaging of local membrane electric fields during the excitation of single neurons in culture. *Biophys. J.* 69:299–310.
15. Huser, J., C. E. Rechenmacher, and L. A. Blatter. 1998. Imaging the permeability pore transition in single mitochondria. *Biophys. J.* 74: 2129–2137.
16. Bai, G., K. V. R. Rao, C. R. K. Murthy, K. S. Panickar, A. R. Jayakumar, and M. D. Norenberg. 2001. Ammonia induces the mitochondrial permeability transition in primary cultures of rat astrocytes. *J. Neurosci. Res.* 66:981–991.
17. Cesura, A. M., E. Pinard, R. Schubenel, V. Goetschy, A. Friedlein, H. Langen, P. Polcic, M. A. Forte, P. Bernardi, and J. A. Kemp. 2003. The voltage-dependent anion channel is the target for a new class of inhibitors of the mitochondrial permeability transition pore. *J. Biochem. (Tokyo).* 278:49812–49818.
18. Cohen, L. B., B. M. Salzberg, H. V. Davila, W. N. Ross, D. Landowne, A. S. Waggoner, and C. H. Wang. 1974. Changes in axon fluorescence during activity: molecular probes of membrane potential. *J. Membr. Biol.* 19:1–36.
19. Wu, J. Y., Y. W. Lam, C. X. Falk, L. B. Cohen, J. Fang, L. Loew, J. C. Prechtl, D. Kleinfeld, and Y. Tsau. 1998. Voltage-sensitive dyes for monitoring multineuronal activity in the intact central nervous system. *Histochem. J.* 30:169–187.

20. Briggman, K. L., H. D. I. Abarbanel, and W. B. Kristan. 2005. Optical imaging of neuronal populations during decision-making. *Science*. 307: 896–901.

21. Lehmann-Horn, F., and K. Jurkat-Rott. 2003. Nanotechnology for neuronal ion channels. *J. Neurol. Neurosurg. Psychiatry*. 74:1466–1475.

22. Siegel, M. S., and E. Y. Isacoff. 2005. Green fluorescent proteins for measuring voltage. *In* Imaging in Neuroscience and Development: A Laboratory Manual. R. Yuste and A. Konnerth, editors. Cold Spring Harbor Laboratory Press, Cold Spring Harbor, NY. 573–578.

23. Kuznetsov, A., V. P. Bindokas, J. D. Marks, and L. H. Philipson. 2005. FRET-based voltage probes for confocal imaging: membrane potential oscillations throughout pancreatic islets. *Am. J. Physiol. Cell Physiol.* 289:224–229.

24. Mazzanti, M., J. O. Bustamante, and H. Oberleithner. 2001. Electrical dimension of the nuclear envelope. *Physiol. Rev.* 81:1–19.

25. Gross, D., L. M. Lowe, and W. W. Webb. 1986. Optical imaging of cell membrane potential changes induced by applied electric fields. *Biophys. J.* 50:339–348.

26. Bullen, A., and P. Saggau. 1999. High-speed, random-access fluorescence microscopy: II. Fast quantitative measurements with voltage-sensitive dyes. *Biophys. J.* 76:2272–2282.

27. Buck, S. M., H. Xu, M. Brasuel, M. A. Philbert, and R. Kopelman. 2004. Nanoscale probes encapsulated by biologically localized embedding (PEBBLES) for ion sensing and imaging in live cells. *Talanta*. 63:41–59.

28. Behrend, C. J., J. N. Anker, B. H. McNaughton, and R. Kopelman. 2005. Microrheology with modulated optical nanoprobes (MOONs). *J. Magn. Magn. Mater.* 293:663–670.

29. Loew, L. M. 1996. Potentiometric dyes: imaging electrical activity of cell membranes. *Pure Appl. Chem.* 68:1405–1409.

30. Knisley, S. B., R. K. Justice, W. Kong, and P. L. Johnson. 2000. Ratiometry of transmembrane voltage-sensitive fluorescent dye emission in hearts. *Am. J. Physiol. Heart Circ. Physiol.* 279:1421–1433.

31. Polymicro Technologies. 2005. Quartz/Silica Characteristics—Typical Electrical Properties. http://www.polymicro.com/catalog/A_10.htm.

32. Radany, E. H., M. Brenner, F. Besnard, V. Bigornia, J. M. Bishop, and C. F. Deschepper. 1992. Directed establishment of rat brain cell lines with the phenotypic characteristics of type 1 astrocytes. *P. Natl. Acad. Sci. USA*. 89:6467–6471.

33. Das, S., T. K. Jain, and A. Maitra. 2002. Inorganic-organic hybrid nanoparticles from n-octyl triethoxy silane. *J. Colloid Interf. Sci.* 252:82–88.

34. Fluhler, E., V. G. Burnham, and L. M. Loew. 1985. Spectra, membrane binding, and potentiometric responses of new charge shift probes. *Biochemistry*. 24:5749–5755.

35. Clark, R. M., and D. J. Kane. 1997. Optical detection of membrane dipole potential: avoidance of fluidity and dye-induced effects. *Biochim. Biophys. Acta*. 1323:223–238.

36. Clark, R. J., P. Schrimpf, and M. Schoneich. 1992. Spectroscopic investigations of the potential-sensitive membrane probe RH421. *Biochim. Biophys. Acta*. 1112:142–152.

37. Krammer, B. E. 1996. Microelectrode recordings of the transmembrane potential of the nucleus and the cytoplasm in living human fibroblasts. *Bioelectrochem. Bioenerg.* 40:67–70.

38. Kamp, F., Y. D. Chen, and H. V. Westerhoff. 1988. Energization-induced redistribution of charge carriers near membranes. *Biophys. Chem.* 30:113–132.

39. Olivotto, M., A. Arcangeli, M. Carla, and E. Wanke. 1996. Electric fields at the plasma membrane level: a neglected element in the mechanisms of cell signaling. *Bioessays*. 18:495–504.

40. Pollack, G. H. 2003. The role of aqueous interfaces in the cell. *Adv. Colloid. Interface Sci.* 103:173–196.

41. Zheng, J. M., and G. H. Pollack. 2003. Long-range forces extending from polymer-gel surfaces. *Phys. Rev. E*. 68:1–7.

42. Priel, A., A. J. Ramos, J. A. Tuszynski, and H. F. Cantiello. 2006. A bio-polymer transistor: electrical amplification by microtubules. *Biophys. J.* 90:4639–4643.

43. Tuszynski, J. A., S. Portet, J. M. Dixon, C. Luxford, and H. F. Cantiello. 2004. Ionic wave propagation along actin filaments. *Biophys. J.* 86:1890–1903.